

MODELING THE QUENCHING OF A CALANDRIA TUBE FOLLOWING A CRITICAL BREAK LOCA IN A CANDU REACTOR

J. T. Jiang and J. C. Luxat

Department of Engineering Physics
McMaster University

ABSTRACT.

Following a postulated critical large break LOCA a pressure tube (PT) can experience creep deformation and balloon uniformly into contact with the calandria tube (CT). The resultant heat flux to CT is high as stored heat is transferred out of the hot PT. This heat flux can cause dryout on the outer surface of the CT and establish film boiling. This paper presents a model of buoyancy-driven natural convection film boiling on the outside of a horizontal tube with diameter relevant to a CANDU CT (approximately 130mm). The model has been developed to analyze the variation of steady state vapor film thickness as a function of sub-cooling temperature, wall superheat and incident heat flux. The CT outer surface heat flux and effective film boiling heat transfer coefficient from the model are in good agreement with available experimental data.

1. INTRODUCTION

The Canada Deuterium Uranium (CANDU) reactor core consists of several hundred horizontal fuel channels. Each fuel channel is comprised of a pressure tube, containing fuel bundles, within a concentric calandria tube separated from the pressure tube by a gas filled annulus. Calandria tubes are surrounded by the heavy-water moderator. In a postulated critical large break loss of coolant accident (LBLOCA) it is possible that heatup of a PT can occur to the extent that creep deformation of the pressure tube occurs. If the internal pressure is sufficiently high then uniform ballooning deformation forces the hot pressure tube into contact with the CT. Following the contact of the hot pressure tube with the CT, there is a high heat flux into the CT as stored heat is transferred out of the PT. This high heat flux can cause dryout of the CT and establishment of film boiling on the outer surface of the tube. The safety concern associated with this condition is that if the temperature of the CT experiencing film boiling gets sufficiently high, then failure of the fuel channel may occur. However, quench heat transfer can limit the extent and duration of film boiling, as has been experimentally observed. Current estimates of quench temperature during pool film boiling are primarily based on experimental correlations. Given a set of specific thermal-hydraulic parameters, there exists a critical vapor film thickness. This film thicknesses can be used to demarcate the conditions under which the vapor film is destabilized and a rapid quench is initiated, and consequently fuel channel failure will not occur.

There are neither applicable experimental measurements associated with stable vapor film thicknesses and critical vapor film thicknesses in the open literature, nor relevant film thickness calculations associated with the CANDU CT configuration. This paper considers film boiling at

the stagnation-point on a horizontally orientated tube (130 mm in diameter) submerged in sub-cooled heavy water without forced cross flow. An expression for vapor evaporation velocity is derived from heat balance considerations. A solution is derived by modifying Bradfield's approach to film-boiling on a down-faced semispherical end of a vertically orientated tube [1].

2. THEORETICAL DERIVATION

2.1 Model Description and Assumptions

Film boiling on a horizontal CT is characterized by the existence of a continuous vapor film surrounding the heated CT outer surface. The region of the stagnation point at the lowest part of the CT is dominated by mass transfer. Continuous vapor formation sustains a vapor blanket along the CT outer surface. Vapor departs from the upper part of the cylinder, as showed in Figure 1. The vapor transient separation angle, ξ_v , indicates the position at which the vapor transitions from laminar to turbulent flow. Similarly, there exists a liquid transient separation angle, ξ_L , in the liquid zone.

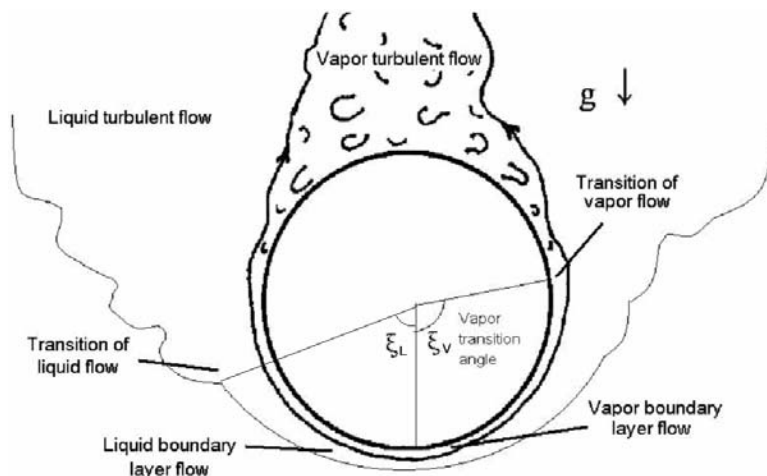


Figure 1: Cross-section of CT experiencing laminar film boiling

The following assumptions are made:

- (1) Incompressible homogeneous liquid and vapor
- (2) Vapor film is very thin with comparison to the radius of CT ($\delta \ll R$)
- (3) Inertial and convection effects in the vapor are negligible
- (4) Viscous dissipation in the vapor film is negligible
- (5) Vapor density is uniformly distributed
- (6) Thermophysical properties of either vapor or liquid are uniform and are temperature dependent
- (7) Thermophysical properties are evaluated at atmospheric pressure
- (8) CT surface temperature are uniform; there is neither circumferential heat loss nor

longitudinal heat loss at the film boiling and quenching spots

- (9) Laminar vapor flow covers most of the CT surface
- (10) Laminar liquid flow develops at the outside of the liquid-vapor interface
- (11) Heat conduction from liquid-vapor interface to subcooled liquid occurs on a thin liquid boundary layer near the liquid-vapor interface
- (12) Smooth liquid-vapor interface
- (13) In the vicinity of stagnation point ($\theta < 5^\circ$) (refer to Fig.2), the variation in vapor film thicknesses are negligible

The cylindrical polar coordinate system given in Figure 2 is appropriate for this geometric configuration. The reference point is taken at the bottom of the CT. A z vector is shown as positively downward along the radial axis and an r vector is tangential to the cylinder surface. The stagnation point is located at the lowest point of the vapor-liquid interface just beneath the original point. $P_{stag}(0, \delta)$ is the liquid side static pressure at the stagnation point and P_{dyn} is the liquid side dynamic pressure at the interface. The angle θ is the azimuthal angle measured in the cylindrical coordinate system. The velocity components u and v are the radial and tangential components, respectively. At position $z = \delta$ from the reference point (the bottom of the cylinder), there is a vapor-liquid interface and the vapor pressure p_v must match the liquid side P_{dyn} .

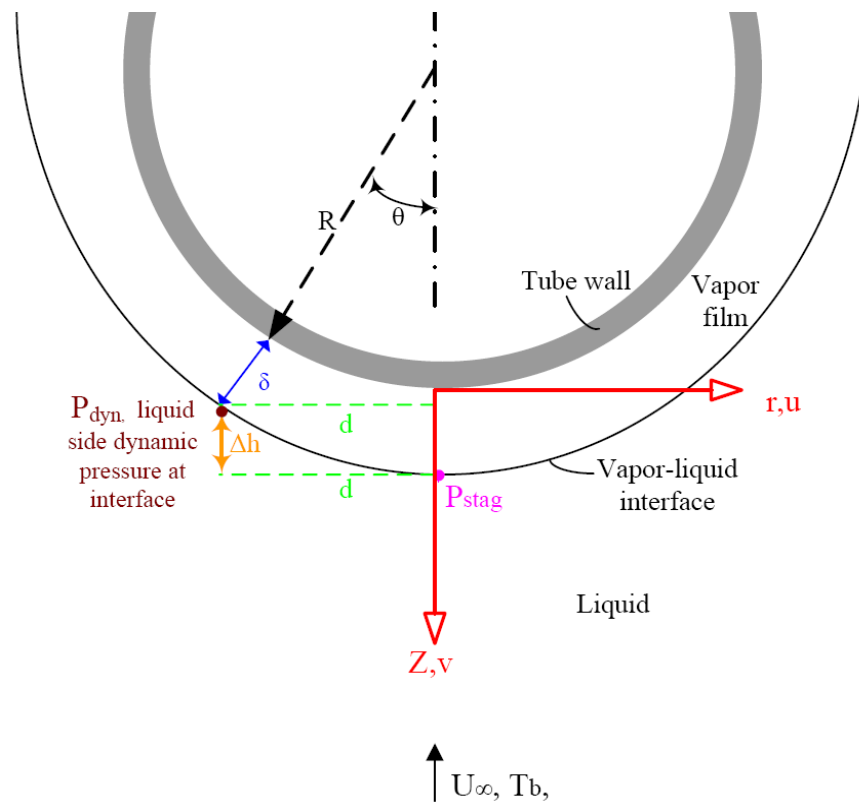


Fig.2: Calandria Tube Geometry and Vapor Film

2.2 Heat Balance and Vaporization Velocity

As shown in Fig.3, all heat transferred from the outside of calandria tube is balanced by two heat transfer components, namely radiation heat transfer to the bulk liquid and the conduction heat transfer across the vapor film. The conduction heat transfer through vapor film heats the vapor film region. This heat transfer is indicated as q''_{sh} in Fig.3. At the liquid-vapor interface part of the conduction heat evaporates liquid to maintain the vapor film; while the remainder of the conduction heat is transferred to the bulk liquid by convection. The definition of symbols in Figure 3 are listed in the nomenclature.

The heat balance at the calandria tube wall can be written as

$$q''_{co} = q''_r + q''_c \quad (1)$$

and the heat balance at the liquid-vapor interface is:

$$q''_c = q''_{evap} + q''_{sh} + q''_{i-L} \quad (2)$$

The total heat flux at the CT outside surface, q''_{co} , is comprised of radiation heat flux (q''_r) and conduction heat flux (q''_c). The portion of the conduction heat flux that superheats the vapor film is q''_{sh} . The component of conduction heat transfer that vaporizes saturated liquid at the interface is denoted as q''_{evap} . The heat transferred away from the interface to the bulk liquid is denoted as q''_{i-L} .

The heat conducted from the vapor-liquid interface to bulk liquid can be treated by Sidman's equivalence theory [2] that is based on potential flow and also on the notion that the heat transfer in the liquid is confined to a thin layer near the vapor-liquid interface. Witte [3] developed an expression based upon the temperature gradient for a horizontal cylinder and has the following form:

$$\left. \frac{\partial T_L}{\partial z} \right)_{z=\delta} = -\sqrt{\frac{2 U_\infty}{\pi R \alpha_L (1 - \cos \theta)}} \cdot \sin \theta \cdot \Delta T_{sub}$$

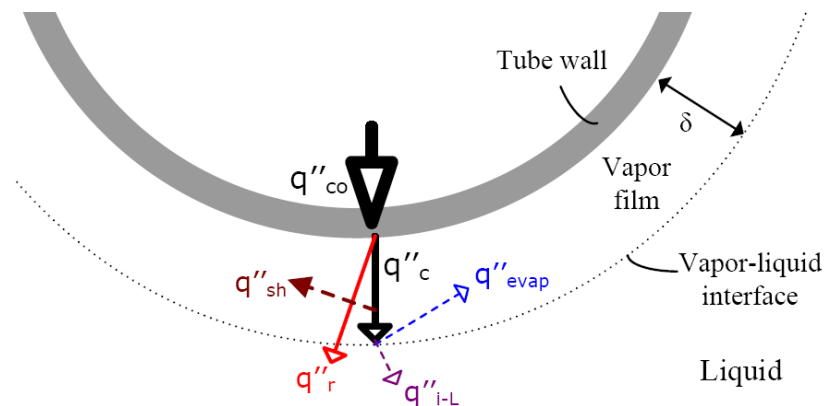


Fig.3: Model of film-boiling heat transfer mechanism

Therefore, the conduction heat flux from the vapor-liquid interface to the subcooled thin liquid

layer is

$$q''_{i-L} = -k_L \left. \frac{\partial T_L}{\partial z} \right|_{z=\delta} = 2k_L \sqrt{\frac{U_\infty}{\pi R \alpha_L}} \cdot \cos \frac{\theta}{2} \cdot \Delta T_{sub} \quad (3)$$

In the region of stagnation point, i.e. as $\theta \rightarrow 0$, equation (3) becomes

$$q''_{i-L} = -k_L \left. \frac{\partial T_L}{\partial z} \right|_{z=\delta, \theta=0} = 2k_L \sqrt{\frac{U_\infty}{\pi R \alpha_L}} \cdot \Delta T_{sub} \quad (4)$$

The vapor superheating heat flux can be approximated as

$$q''_{sh} = \rho_v V_{evap} c_{p,v} (T_v - T_{sat}) = \rho_v V_{evap} c_{p,v} [(T_w + T_{sat})/2 - T_{sat}] = 0.5 \rho_v V_{evap} c_{p,v} (T_w - T_{sat}) \quad (5)$$

The heat flux associated with liquid vaporization is

$$q''_{evap} = \rho_v V_{evap} h_{fg} \quad (6)$$

And the conduction heat flux is

$$q''_c = \frac{k_v (T_w - T_{sat})}{\delta} \quad (7)$$

Substituting equations (4),(5) (6) and (7) into equation(2) and solving for V_{evap} , yields

$$V_{evap} = \frac{1}{h'_{fg} \rho_v} \left[\frac{k_v (T_w - T_{sat})}{\delta} - \frac{2k_L \cdot \Delta T_{sub}}{\sqrt{\pi R \alpha}} \sqrt{U_\infty} \right] \quad (8)$$

Taking the time derivative of V_{evap} , yields

$$\dot{V}_{evap} = \frac{1}{h'_{fg} \rho_v} \left[-\frac{k_v (T_w - T_{sat}) \dot{\delta}}{\delta^2} - \frac{2k_L \cdot \Delta T_{sub}}{\sqrt{\pi R \alpha}} \frac{\ddot{\delta}}{\sqrt{U_\infty + \dot{\delta}}} \right] \quad (9)$$

2.3 Governing Equations

At the liquid side near the stagnation point, hydrodynamic pressure and hydrostatic pressure are given by the following relationship derived from the theory of potential cross-flow over a cylinder [15]:

$$P_{dyn} = P_{stag} - \rho_L g \Delta h + \rho_L (U_\infty + \dot{\delta})^2 (1 - 4 \sin^2 \theta) / 2 \quad (10)$$

Bradfield [1] proposed an equation describing the motion of the liquid-vapor interface in the neighborhood of the stagnation point as

$$\frac{P_{stag} - \rho_L g \Delta h}{g} \ddot{\delta} = -P_{dyn} + p_v + \frac{2\sigma}{R} \quad (11)$$

Substituting equation(10) into (11) and rearranging, we have

$$p_v = (1 + \frac{\ddot{\delta}}{g})(P_{stag} - \rho_L g \Delta h) + \frac{1}{2} \rho_L (u_\infty + \dot{\delta})^2 (1 - 4 \sin^2 \theta) - \frac{2\sigma}{R}$$

where $\sin \theta = r/(R+\delta)$ and $\Delta h = (R+\delta)(1 - \cos \theta) = [(R+\delta) \sin \theta]^2 / [(R+\delta)(1 + \cos \theta)] \approx r^2 / 2(R+\delta)$ near the stagnation point (Refer to Fig. 2). So

$$\frac{\partial p_v}{\partial r} = - \left[g + \ddot{\delta} + 4 \frac{(U_\infty + \dot{\delta})^2}{R + \delta} \right] \frac{\rho_L r}{R + \delta} \quad (12)$$

The vapor pressure, p_v , can also be evaluated from the Navier-Stokes equations [15], which are

written as
Continuity

$$\frac{1}{r} \frac{\partial}{\partial r} (ru) + \frac{\partial v}{\partial z} = 0 \quad (13)$$

Tangential momentum

$$\rho_v \left(\frac{\partial u}{\partial t} + u \frac{\partial u}{\partial r} + v \frac{\partial u}{\partial z} \right) = -\frac{\partial p_v}{\partial r} + \mu_v \left[\frac{\partial}{\partial r} \left(\frac{1}{r} \frac{\partial (ru)}{\partial r} \right) + \frac{\partial^2 u}{\partial z^2} \right] \quad (14)$$

Radial momentum

$$\rho_v \left(\frac{\partial v}{\partial t} + u \frac{\partial v}{\partial r} + v \frac{\partial v}{\partial z} \right) = -\frac{\partial p_v}{\partial z} + \mu_v \left[\frac{1}{r} \frac{\partial}{\partial r} \left(r \frac{\partial v}{\partial r} \right) + \frac{\partial^2 v}{\partial z^2} \right] \quad (15)$$

Boundary Conditions

$$\text{At } r = 0: \quad u = 0, \quad (16)$$

$$\text{At } z = 0: \quad u = 0, \quad v = 0, \quad (17)$$

$$\text{At } r=0 \text{ and } z=\delta: \quad u=0, \quad v=\dot{\delta} - V_{evap} \quad (18)$$

2.4 Solution of the Equation

Introducing a function $\Phi(t)$ that satisfies Boundary Condition (17) so that $\Phi(t)=v/z$, an integrating continuity equation (13) yields $u = -\frac{1}{2} r \Phi(t)$. Substituting u into the momentum equation and integrating (14) and (15) with respect to r and z , respectively, the following equation is obtained:

$$p_v = -\rho \left(\frac{1}{2} z^2 - \frac{1}{4} r^2 \right) \frac{\partial \Phi}{\partial t} - \rho \left(\frac{1}{2} z^2 + \frac{1}{8} r^2 \right) \Phi^2 + F(t) \quad (19)$$

where $F(t)$ is an arbitrary function of t . The derivative of p_v with respect to r is

$$\frac{\partial p_v}{\partial r} = -2\rho_v r \left(-\frac{1}{4} \frac{\partial \Phi}{\partial t} + \frac{1}{8} \Phi^2 \right) \quad (20)$$

Applying boundary condition(18) to equation (20) results in

$$\left. \frac{\partial \Phi}{\partial t} \right|_{z=\delta} = \frac{(\ddot{\delta} - \dot{V}_{evap})\delta - (\dot{\delta} - V_{evap})\dot{\delta}}{\delta^2} \quad (21)$$

and

$$\left. \Phi^2 \right|_{z=\delta} = \frac{(\dot{\delta} - V_{evap})^2}{\delta^2} \quad (22)$$

Substituting Equation (8), (9), (21) and (22) into (20) and equating the resultant equation with Equation (12), yields

$$\langle 1 \rangle + \langle 2 \rangle + \langle 3 \rangle + \langle 4 \rangle + \langle 5 \rangle + \langle 6 \rangle + \langle 7 \rangle + \langle 8 \rangle = 0 \quad (23)$$

where

$$\langle 1 \rangle = \ddot{\delta} \left[1 + \frac{\chi(R+\delta)}{\delta} + \frac{1}{2} \chi C_1 \frac{R+\delta}{\delta \sqrt{U_\infty + \delta}} \right], \quad \langle 2 \rangle = \left(\frac{\dot{\delta}}{\delta} \right)^2 \left[-\frac{3}{4} \chi(R+\delta) \right],$$

$$\langle 3 \rangle = \frac{\dot{\delta}}{\delta^2} \left[-2C_1(R+\delta)\sqrt{U_\infty + \delta} \right], \quad \langle 4 \rangle = \frac{\dot{\delta}}{\delta^3} \left[\frac{3}{2} \chi C_2(R+\delta) \right],$$

$$\langle 5 \rangle = \frac{1}{\delta^2} \left[-\chi C_1^2(R+\delta)(U_\infty + \delta) \right], \quad \langle 6 \rangle = \frac{1}{\delta^3} \left[\chi C_1 C_2(R+\delta)(U_\infty + \delta) \right],$$

$$\langle 7 \rangle = \frac{1}{\delta^4} \left[-\frac{1}{4} \chi C_2^2 (R + \delta) \right], \quad \langle 8 \rangle = g(R + \delta) + 4(U_\infty + \delta)^2$$

In the terms above, χ , C_1 and C_2 are defined as, respectively,

$$\chi = \frac{\rho_v}{\rho_L}, \quad C_1 = \frac{k_L \Delta T_{sub}}{h'_{fg} \rho_v \sqrt{\pi R \alpha_L}}, \quad C_2 = \frac{k_v (T_w - T_{sat})}{h'_{fg} \rho_v}.$$

Assigning $\ddot{\delta} = \dot{\delta} = 0$ in Equation (25) yields an equation representing steady state vapor film thickness as,

$$\frac{1}{\delta^2} \left[-\chi C_1^2 U_\infty \right] + \frac{1}{\delta^3} \left[\chi C_1 C_2 U_\infty \right] + \frac{1}{\delta^4} \left[-\frac{1}{4} \chi C_2^2 \right] + g + \frac{4U_\infty^2}{R + \delta} = 0 \quad (24)$$

To evaluate Equation(24), we need to know the liquid free stream velocity, U_∞ .

2.5 Liquid Free Stream Velocity

The liquid free stream velocity, U_∞ , is dominated by two components, namely the liquid phase buoyancy-driven flow and the relative bubble rise velocity of vapor in liquid. The buoyancy-driven flow arises from the temperature-dependent density gradient between the liquid surrounding the cylinder and the bulk liquid and it is a function of liquid subcooling temperature. The bubble rise velocity is dependent upon the vapor bubble size. The effective free steam velocity is given by:

$$U_\infty = U_{sub}(\Delta T_{sub}) + U_{br}(R_b)$$

The effect of bubble rise is an effective increase in the relative velocity at the vapor-liquid interface. The bubble-rise velocity is evaluated from Wallis [4] as

$$U_{br} = 1.00 \sqrt{g R_b}$$

where R_b is the bubble radius. Assuming the characteristic size of the vapor bubble R_b is the calandria tube radius we have $U_{br} = 0.8$ m/s.

As per $U_{sub} = f(\Delta T_{sub})$, we can write down the conservation equations for the liquid laminar boundary layer in a Cartesian coordinate system shown in Fig.4. Applying Schlichting's [16] boundary layer approximations and the Boussinesq approximation [17], the following equation is derived:

$$\frac{d^2 u}{dy^2} \approx -\frac{\rho_L \beta g}{\mu_L} (T_{sat} - T_\infty)$$

Integrating twice yields

$$U_{sub} = \frac{1}{2} \frac{\rho_L \beta g}{\mu_L} (2\delta_L y - y^2) \Delta T_{sub} + C \quad (25)$$

where δ_L is the laminar liquid boundary-layer thickness and C is a constant equal to zero. Applying the Blasius's solution for laminar boundary layer [5], δ_L can be evaluated for a quasi-laminar flow, and is given as

$$\delta_L = \frac{5.0 \xi R}{\sqrt{Re_\xi}}$$

where the local Reynolds number (Re_ξ) is evaluated at the liquid separation angle, ξ_L (Refer to Fig.1). At the conditions $\Delta T_{sub}=20^\circ\text{C}$, $\xi_L=3/4\pi$, and letting $y=\delta_L$, yields $U_{sub} = 0.023\Delta T_{sub}$. Therefore, the free stream velocity can be expressed as $U_\infty = 0.023\Delta T_{sub} + 0.80$ with units of m/s.

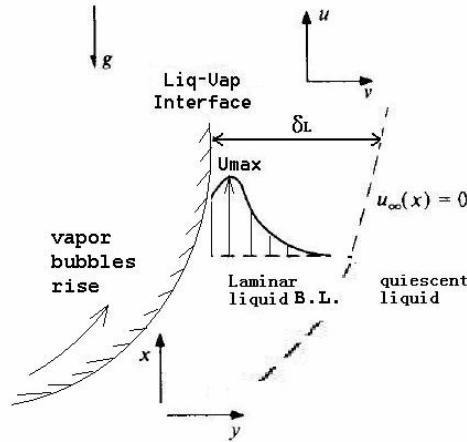


Fig.4: Free stream velocity affected by subcooling

2.6 Lower bound of vapor film thickness

It is of interest to find the lower bound of vapor film thickness which is relevant to the critical thickness of the vapor film prior to a quench. It can be derived from equation (8) with $V_{evap}=0$. This condition implies that the vapor film is no longer stable and continuously decreases due to cessation of vapor generation until liquid rewets the wall surface. A relationship between the calandria tube wall temperature and the subcooling is then established as,

$$T_w = T_{sat} + \frac{2k_L}{k_v \sqrt{\pi R \alpha_L}} \sqrt{U_\infty} \delta \cdot \Delta T_{sub} \quad (26)$$

Equation (24) and (26) are used to evaluate the lower bound vapor film thickness in terms of a number of key thermalhydraulic parameters which are varied in order to investigate their effect on the vapor film thickness.

3. RESULTS and DISCUSSIONS

3.1 Vapor Film Thickness as a Function of Key Parameters

As shown in Fig.6 and Fig.7, the vapor film thickness decreases as the incident heat flux decrease. The same tendency of vapor film thickness decrease is exhibited by a decrease in the calandria tube surface temperature. Vapor film thickness decreases with increase in subcooling temperature, as might be expected.

3.2 Quench or No Quench

Fig.8 presents a curve that demarcates a boundary between quench and no quench of the CT outside surface based upon the relationship between vapor film thickness and the heat conducted in the vapor film. A quench will initiate at heat fluxes below the line, while heat fluxes above the line are likely to maintain stable film boiling.

In Fig.9 CT wall heat fluxes below the line will lead to quenching of the CT wall surface due to an inability to maintain a stable vapor film. Conversely, at heat fluxes above the line are likely to result in formation of a stable vapor film and probable dryout of the CT surface. As indicated in Fig.9 higher heat fluxes on the CT wall are required for film boiling when the bulk liquid subcooling temperature increases.

3.3 Heat Flux Contribution

Fig.10 shows the fractional contribution of the radiation and conduction heat transfer components of the total heat out of the calandria tube outside surface as a function of liquid subcooling at conditions where a quench is about to be initiated. Both components are essentially independent of liquid subcooling with radiation heat transfer contributing around 4% and conduction heat transfer contributing 96% of the total heat transfer from CT outside surface.

Fig.11 shows that the majority of heat transferred to the vapor-liquid interface is used to vaporize saturated liquid to maintain vapor film-boiling. With increase in subcooling from 0°C to 50°C, the percentage of vaporization heat drops from 90% to 73%. During this process the contribution of heat to super-heat the vapor region gradually increases to 18% at 50°C subcooling from 9% at 0°C subcooling. The interface-to-liquid heat transfer also gradually increases from 0% at 0°C subcooling to 10% at 50°C subcooling.

3.4 Comparison to Available Experimental Data

Three plots shown in Figures 12, 13 and 14, generated from application of the model to evaluate CT quench behavior, are compared to data from the open literature and to contact boiling test data. In Fig.12 the solid line represents the heat flux on the calandria tube outside surface obtained from the model, while the dotted line is obtained by converting the heatup rates [6] of the pressure tube to equivalent heat fluxes on the calandria tube outside surface. The model underestimates heat fluxes at quench by 2.2% over the subcooling range from 0°C to 30°C. At higher subcooling up to 50°C the model underestimation of quench heat flux increases to a maximum of 5%. The agreement between the model and the experimental data is considered to be good.

Fig.13 compares the effective film-boiling heat transfer coefficient derived from the model with the Gillespie & Moyer correlation [7], given by $h_{fb}=0.2(1+0.031*\Delta T_{sub})$ [kW/(m²°C)]. A relatively constant 7% overprediction by the model occurs for all subcoolings. This difference is not surprising since the Gillespie & Moyer correlation is defined for stable film-boiling, whereas the model predicts the conditions for onset of quench and is therefore expected to yield a somewhat

higher heat transfer coefficient. The transition from stable film-boiling to quench is associated with an unstable reduction in the vapor film thickness. The conduction heat flux, $k_v(T_w - T_{sat})/\delta$, will increase due to the reduction of vapor film thickness. As shown in Fig.10, approximately 96% of heat transfer from the CT wall is due to conduction through the vapor film and any increase in conduction heat flux ultimately results in a higher effective heat transfer coefficient at quench than that at stable film-boiling. This behaviour is expected to occur at all subcoolings.

At the evaluated quench heat fluxes the model can also predict the wall temperature of the calandria tube at quench initiation. Several empirical correlations for minimum film-boiling temperature, T_{mfb} , from open literatures are plotted in Fig.14, as well as the values predicted by the model. The empirical correlations at atmospheric pressure with a unit of °C are listed below:

- Ohnishi [8]: $T_{mfb} = 5.1\Delta T_{sub} + 450$
- Bradfield [9]: $T_{mfb} = 6.15\Delta T_{sub} + 300$
- Groeneveld & Stewart [10]: $T_{mfb} = 6.3\Delta T_{sub} + 389$
- Adler [11]: $T_{mfb} = 7\Delta T_{sub} + 275$
- Mori [12]: $T_{mfb} = 7.5\Delta T_{sub} + 240$
- Lauer [18]/COG experiment: $T_{mfb} = 5.893\Delta T_{sub} + 328.6$

The model predictions are in general agreement with the majority of the correlations and are higher than the lower bound Mori correlation over most of the subcooling range. The quench temperatures predicted from the model are lower than the quench temperatures inferred from the contact boiling experimental data with a maximum underprediction of 41°C at a subcooling of 10°C. The following four reasons may possibly account for this difference.

- (1) As mentioned by Carbajo [13], the minimum film boiling temperature differs from the quench temperature. Due to the installation locations of the thermal couples being a certain distance away under the CT surface, the measured temperature may be higher than the instantaneous quench temperature.
- (2) The definition of quench temperature may vary with individual judgments. There are two ways of defining quench temperature prevails over others. Point A in Fig.5 corresponds to the temperature at which an increase in negative slope of the temperature transient is observable. Point B is a projected temperature based on the intersection of the two distinct slopes in the temperature transient. The experimenters above may refer to Point A for their correlations. The model predicted the quench temperatures are very likely close to the temperature at Point B, based on the definition of the evaporation velocity being zero at quench initiation.
- (3) The geometry has influence on the quench temperature. It was reported [14] that small diameter heaters have higher T_{mfb} and higher quench temperature than large heaters do. The correlations above are based on tube data and the tubes are smaller than CANDU calandria tube.

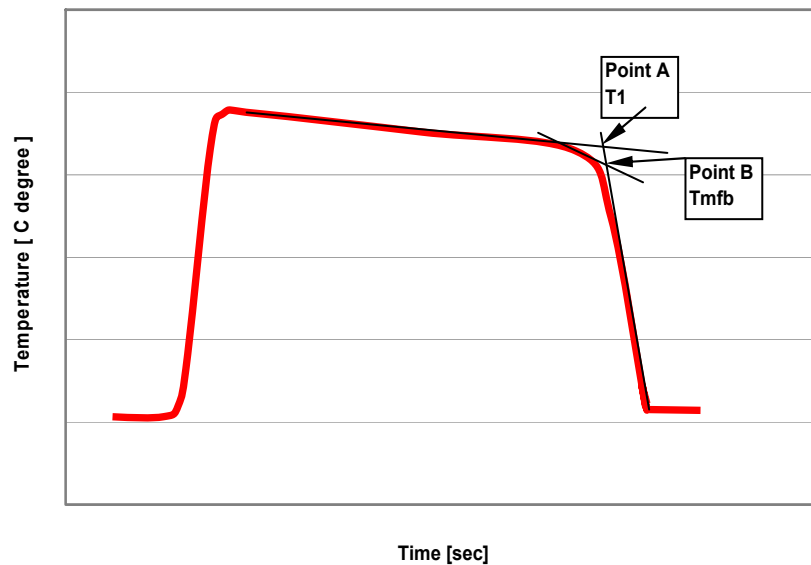


Fig.5: A typical quench curve transient [6]

- (4) Surface conditions, such as surface roughness and oxidization, affect the T_{mfb} or quench temperature as well. The surface conditions were not mentioned in some correlations above. In the model, the non-oxidized Zircaloy with emissivity of 0.2 was used. In general, both T_{mfb} and quench temperature increase as the surface becomes oxidized.

Overall, the model predictions are most similar to Groeneveld & Stewart's correlation.

4. CONCLUSIONS

The conclusions drawn from the modeling of pool film-boiling and quenching on the outside of a CT are as follows:

- The proposed model provides an understanding of the influence of thermohydraulic parameters on the film-boiling heat transfer.
- Vapor film thicknesses can be calculated at given conditions.
- The model clearly demarcated the requirements for the occurrence of quench
- A relationship between quench temperature and subcooling is provided which is close to Bradfield's correlation for minimum film-boiling temperature.
- The model matches available experimental data quite well. The accuracy of predictions by the model is summarized in Table 1 below.

5. FUTURE TASKS

The current conclusions are based on the quench conditions applied to steady-state conditions. The transient equation (23) needs to be solved to address potential instabilities at the liquid-vapor interface when quenching is initiated. Further study will elucidate the impact of transient changes in key parameters, such as subcooling, wall heat flux etc., on the stable-film boiling.

Table 1: Error % in Prediction

	ΔT_{sub}										
	0°C	5°C	10°C	15°C	20°C	25°C	30°C	35°C	40°C	45°C	50°C
Error % in Prediction of CT Wall Heat Flux	-1.0	0.7	0.9	0.4	-0.4	-1.3	-2.2	-3.1	-3.8	-4.4	-4.8
Error % in Prediction of Effective film-boiling Heat Transfer Coefficient	1.3	6.13	8.1	8.6	8.4	7.9	7.2	6.6	6.0	5.5	5.2
Error % in Prediction of Calandria tube outside wall temperature	-4.2	-5.9	-6.7	-6.8	-6.5	-6.0	-5.4	-4.6	-3.9	-3.2	-2.5

6. ACKNOWLEDGEMENT

The financial support of the Natural Sciences and Engineering Research Council (NSERC) and the University Network of Excellence in Nuclear Engineering (UNENE) is gratefully acknowledged.

7. NOMENCLATURE

- C = a constant appearing in Equation (25)
- q''_{co} = total heat flux emitted from CT outer surface
- q''_{r} = radiation heat flux from CT wall to bulk liquid
- q''_{sh} = heat flux to superheat steam vapor
- q''_{c} = conduction heat flux from CT wall across vapor film
- q''_{evap} = heat flux used to evaporate saturated liquid
- $q''_{\text{i-L}}$ = heat flux transferred from interface to thin liquid layer
- Q = heat rate
- h_{fg} = latent heat of vaporization
- h'_{fg} = modified latent heat of vaporization = $h_{fg} + 0.5c_{p,v}(T_w - T_{\text{sat}})$
- g = gravity acceleration
- h = effective heat transfer coefficient
- p,P = pressure
- R = calandria tube radius
- T = Temperature

$\Delta T_{\text{sub}}, T_{\text{sub}} =$ subcooling temperature ($=T_{\text{sat}} - T_b$)

$u, v,$ = velocity component along r, z axis in Cylindrical polar coordinate system or along x, y in Cartesian coordinate system, respectively

U, V = velocity

U_{∞} = liquid free stream velocity

α = thermal diffusivity

β = thermal expansion

θ = deflection angle

δ = vapor film thickness

$\dot{\delta}$ = moving velocity of vapor-liquid interface

$\ddot{\delta}$ = the acceleration of vapor-liquid interface

δ_L = thickness of laminar liquid boundary layer

ρ = density

κ = conductivity

μ = dynamic viscosity

ξ = vapor transition angle(from laminar to turbulent flow)

σ = the water surface tension

χ = ratio of vapor density to liquid density (ρ_v/ρ_L)

Φ = a potential function

Subscript:

b = bulk liquid or bubble

br = bubble rise

c, cond = conduction

evap= evaporation

i-L = 2 phase interface to liquid

L = liquid

mfbo = minimum film boiling

r, rad = radiation

sat = saturation condition

sub = subcooling condition

sh = superheating condition

v = vapor

w, wall = wall surface

∞ = liquid free stream condition

8. REFERENCES

- [1] W. S. Bradfield, "Wave Generation at a Stagnation Point in Stable Film Boiling", Report No. 35, Spec TAI.N532, No. 35, C.2, April 1965, College of Engineering, State University of New York At Stony Brook.
- [2] S. Sideman, "The Equivalence of the Penetration and Potential Flow Theories", Industrial and

- Engineering Chemistry, Vol.58, No.2, Feb 1966, pp57 (54-68).
- [3] L.C. Witte, J. Orozco, "The Effect of Vapor Velocity Profile Shape on Flow Film Boiling from Submerged Bodies", ASME Journal of Heat Transfer, Vol.106, Feb 1984, pp193 (191-197).
- [4] G. B. Wallis, "One-dimensional Two-phase Flow", McGraw-Hill, 1969, pp249.
- [5] H. Blasius, "Grenzschichten in Flüssigkeiten mit kleiner Reibung", Z.Math.Phys.vol 56,1908,pp.1-37. <http://naca.larc.nasa.gov/reports/1950/naca-tm-1256> (English translation). Retrieved from "http://en.wikipedia.org/wiki/Blasius_boundary_layer"
- [6] J. C. Luxat, "Mechanistic Modeling of Heat Transfer Processes Governing Pressure Tube-To-Calandria Tube Contact and Fuel Channel Failure", Proceedings CNS Annual Conference, June 2-5, 2002
- [7] G. Gillespie & R. Moyer, "An Experimental Determination of Heat Transfer from large Cylinders: Film Boiling in Subcooled Water", WNRE-569, AECL, February 1984
- [8] N. Ohnishi, K. Ishijima and S. Tanzawa, "A Study of Subcooled Film-Boiling Heat Transfer Under Reactivity-Initiated Accident Conditions in Light Water Reactor", Nuclear Science & Engineering, 88, 331, 1984, pp331-341.
- [9] W. S. Bradfield, "On the Effect of Subcooling on Wall Superheat in Pool Boiling", Trans. ASME, Journal of Heat Transfer, 89-C, 1967.
- [10] L. H. K. Leung and D. Groeneveld (Editors), "Compendium of Thermalhydraulics Correlations and Fluid Properties", Ver. 1991, Revision 1, COG-90-86.
- [11] M. R. Adler, "The Influence of Water Purity and Subcooling on the Minimum Film Boiling Temperature, M. S. thesis, University of Illinois, Urbana-Champaign(1979).
- [12] M. Mori, S. Toda, M. Ochiai, and S. Saito, "Transient Cooling Process of Fuel Rod in Reactivity Initiated Accident, Journal of Nuclear and Science Technology, 17(6), 1980, pp413-424.
- [13] J. J. Carbajo, "A Study of Rewetting Temperatures", Nuclear Engineering and Design, Vol. 84, No.1, Jan.1985.
- [14] F. S. Gunnerson and A. W. Cronenberg, "On the Minimum Film Boiling Conditions for Spherical Geometries", Trans. ASME, Journal of Heat Transfer, 102(1980), pp335-341
- [15] R. Fox, A. T. McDonald and P. J. Pritchard, "Introduction to Fluid Mechanics" 6th ed., Student Resource CD-ROM, S-22. John Wiley & Sons.
- [16] Schlichting, "Boundary Layer Theory", 7th ed, New York, 1979
- [17] F. P. Incropera, D. P. DeWitt, Fundamentals of Heat and Mass Transfer, 5 ed, 2002
- [18] H. Lauer and W. Hufschmidt, "Heat Transfer and Surface Rewet during Quenching", Europe Two-phase Flow Group Meeting at Erlangen, May 31-June 4, 1976

Fig.6: Influence of vapor film thickness increase on CT wall temperature

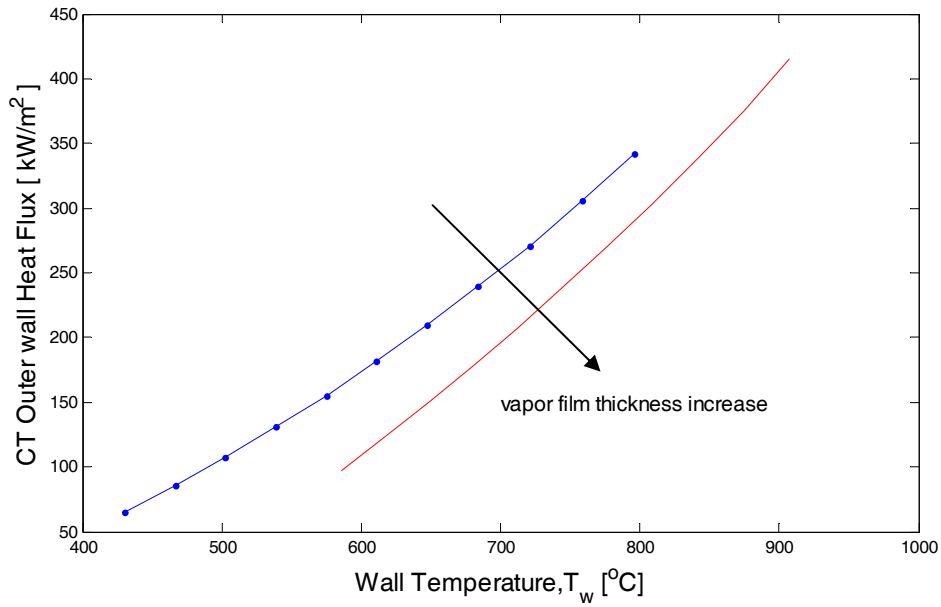


Fig.7: Vapor Film Thickness ($U_{\infty}=0.0233\Delta T_{sub}+0.43$ m/s)

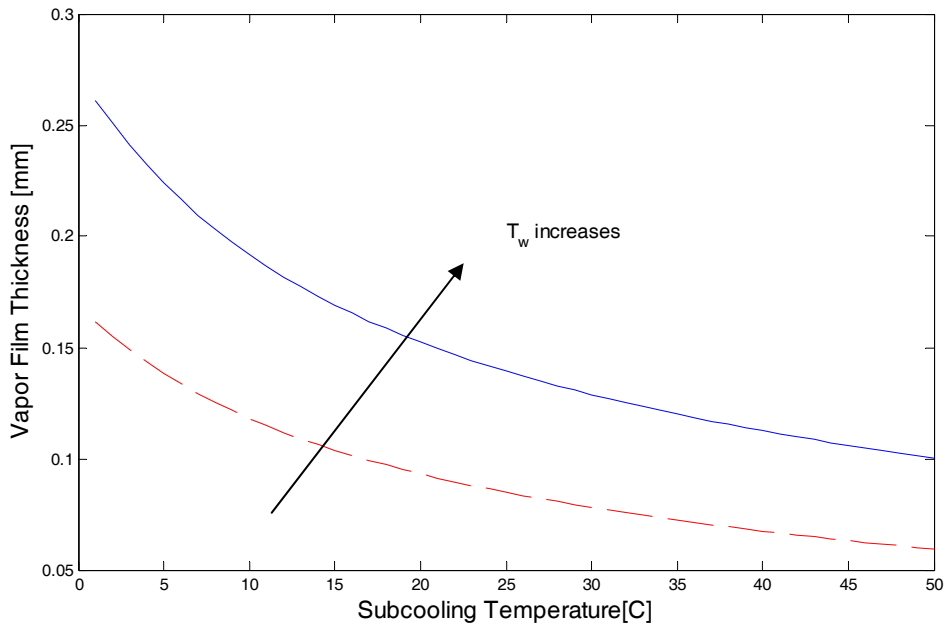


Fig.8: Conduction Heat Flux vs VaporFilm Thickness

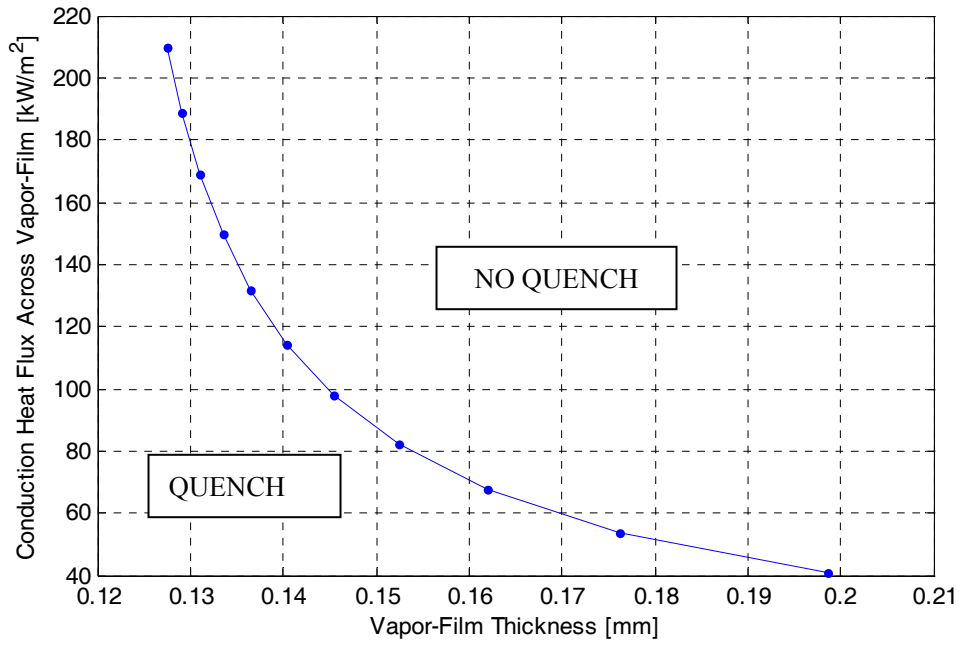


Fig.9: CT outside Surface Heat Flux at Quench vs Subcooling

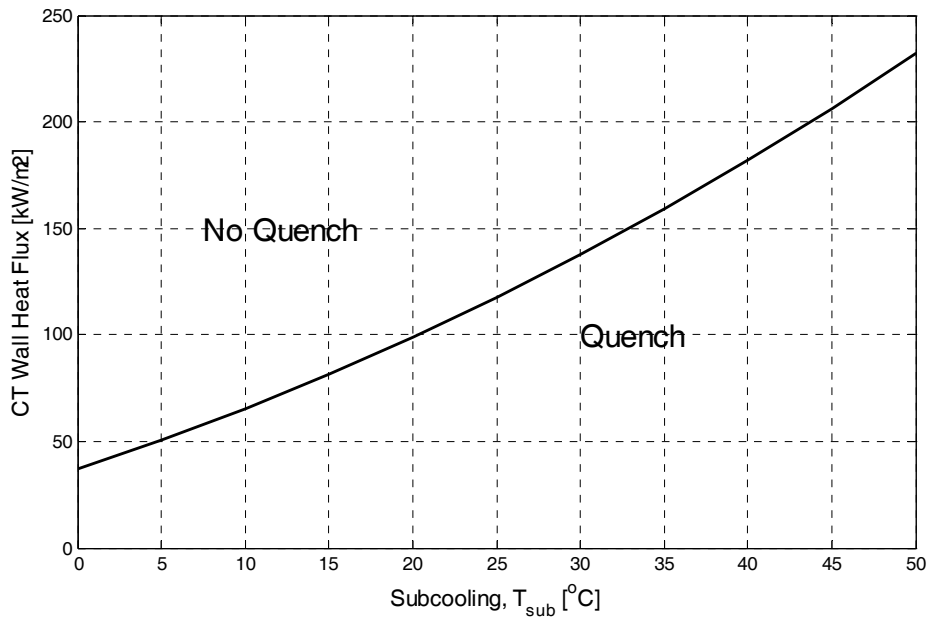


Fig.10: The Contribution of Radiation Heat Flux to the Total CT outside surface Heat Flux

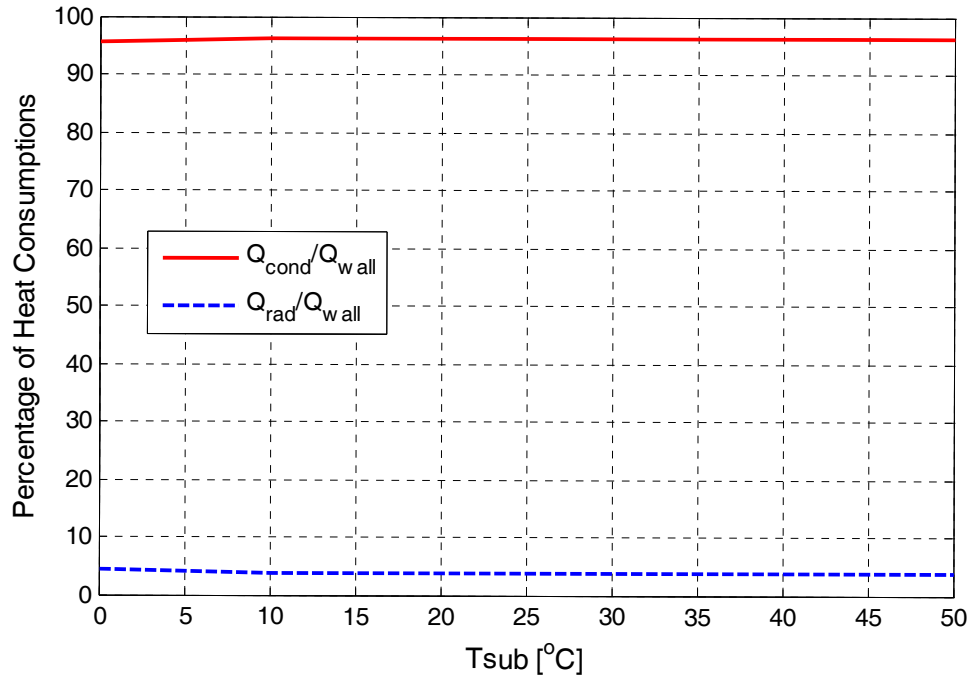


Fig.11: Contribution of evaporation, super-heating and interface-to-liquid heat to the heat conducted through the vapor film

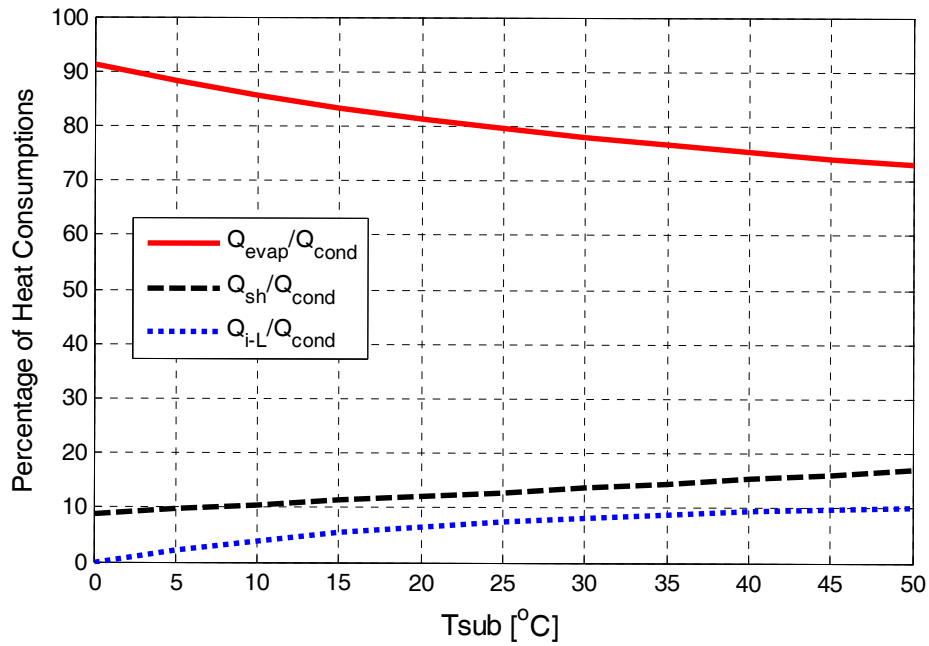


Fig. 12: Prediction of Heat Flux at quench with comparison to COG experimental data

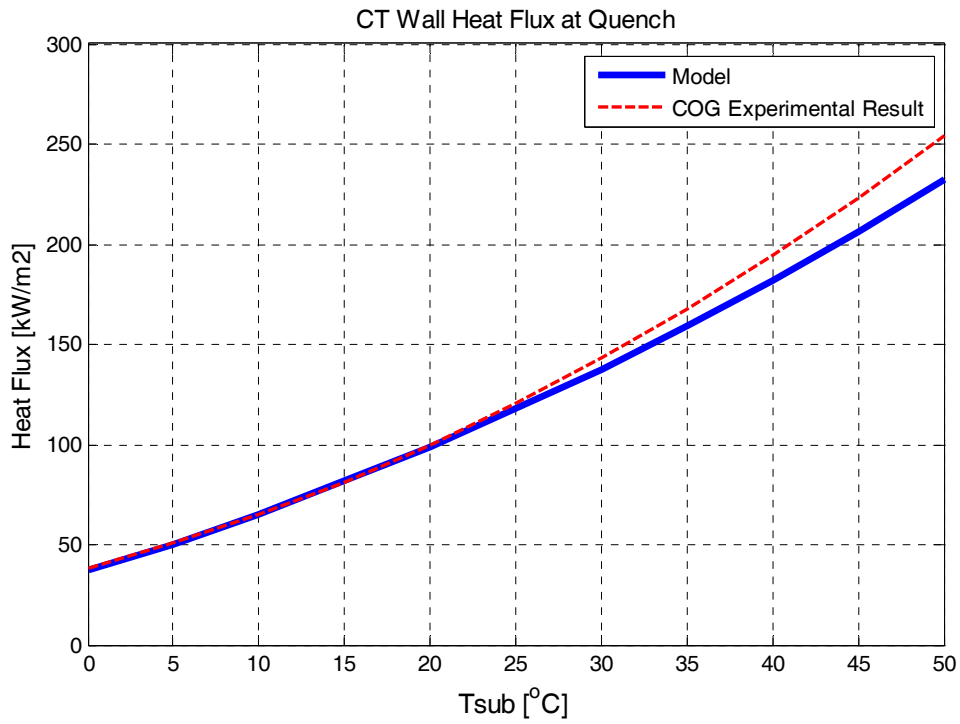


Fig. 13: Prediction on effective film-boiling heat transfer coefficient with comparison to Gillespie & Moyer correlation

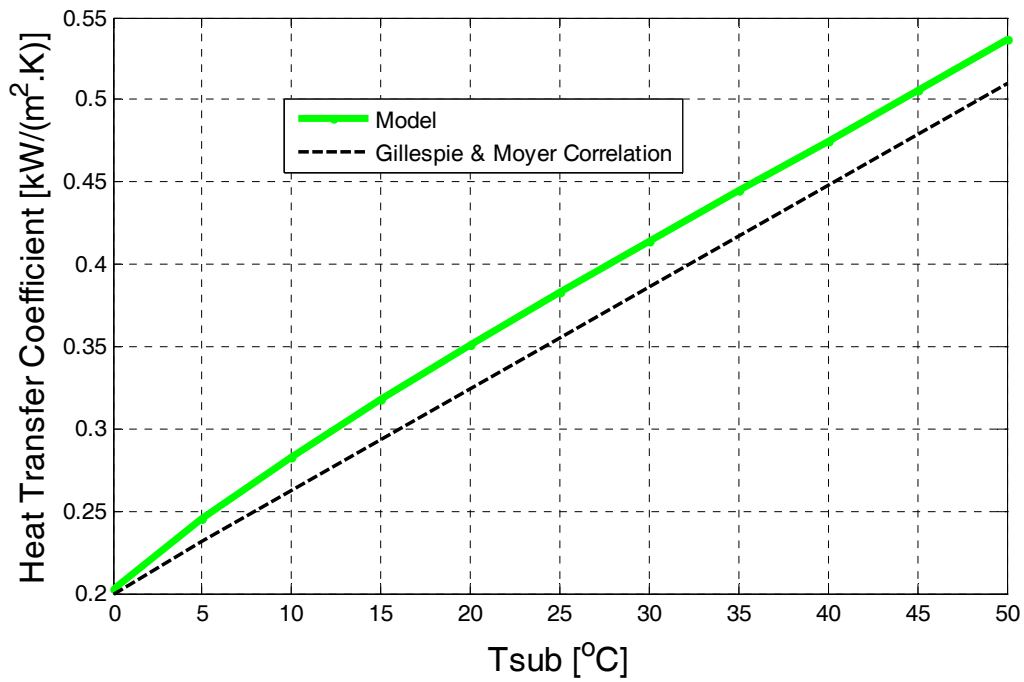


Fig.14: Prediction on minimum film boiling temperature with comparison to existing correlations

